Analysis of BER and Coverage Performance of LoRa Modulation under Same Spreading Factor Interference

Tallal Elshabrawy
Faculty of Information Engineering & Technology
German University in Cairo, Egypt
tallal.el-shabrawy@guc.edu.eg

Joerg Robert
Lehrstuhl für Informationstechnik
(Kommunikationselektronik)
Friedrich-Alexander Universität Erlangen-Nürnberg,
joerg.robert@fau.de

***Abstract*—In the patented LoRa modulation, linearly increasing cyclic chirp signals span the LoRa bandwidth. The rate of increase of these chirp signals is dependent on the applied spreading factor that could vary between 7 and 12. Typically, LoRa signals with different spreading factors are quasi-orthogonal such that LoRa supports multiple simultaneous logical networks. Nevertheless, coverage of LoRa signals may still be maintained under same spreading factor interference provided that the signal of interest satisfies some SNR as well as SIR thresholds. In this paper, numerical approximation of BER performance of LoRa modulation as a function of both SNR and SIR is provided. The advantage of the proposed analysis is that it incorporates the joint impact of SNR and SIR on the coverage probability of LoRa signals exposed to same spreading factor interference. This is contrary to the prevailing approaches in the literature that set independent SNR and SIR thresholds to signify coverage. Comparison between numerical and simulation results shows the high accuracy of the presented approximation. Moreover, simulation of LoRa networks with uniformly distributed end-devices reveals that the approaches adopted in the literature of using a constant SIR threshold of 6 dB to declare coverage may significantly underestimate the coverage probability of LoRa signals under same spreading factor interference.**

***Index Terms*—LP-WAN, LoRa Modulation, Same SF Interference, BER Performance, Coverage Probability.**

I. Introduction

The realization of a multitude of IoT applications particularly within smart cities envisions deployment over Low Power Wide Area Networks (LP-WAN) [1]. LP-WAN are typically configured as star-of-star networks. Within each underlying star network, thousands of power-constrained IoT end-devices communicate directly with an IoT gateway over long distances at the scale of kilometers [1]. LoRa has been exhibiting tremendous commercial growth to establish itself among the front runners of emerging LP-WAN. Pillared on its patented chirp spread spectrum modulation, LoRa supports energy-efficient/reliable long-range communication. In LoRa modulation, linearly increasing cyclic chirp signals span the LoRa bandwidth [2]. The rate of increase of these chirp signals is dependent on the applied spreading factor that can vary between 7 and 12. Increasing the spreading factor extends LoRa coverage range at the expense of a reduced data rate.

LoRa signals with different spreading factors are quasi-orthogonal such that LoRa supports multiple simultaneous logical networks [3]. On the other hand, LoRa signals with the same spreading factor exhibit cross-correlation properties that could make them vulnerable to same spreading factor (same SF) interference. Given that LoRa adopts pure ALOHA for medium access, LoRa signals are inevitably exposed to the threat of same SF interference particulary for dense IoT deployments. The ability of LoRa gateways to maintain coverage for a LoRa signal that is hit by same SF interference has been mainly attributed in the literature to the events when the signal of interest enjoys an SIR that exceeds a given threshold [3], [4], [5], [6]. The SIR threshold has been commonly set to a constant value in isolation of the SNR situation at the signal of interest. In [3], [4], [5], an SIR threshold of $6\,\mathrm{dB}$ has been assumed based on average measurements of communication between two LoRa devices. In [6], an SIR threshold of $0\,\mathrm{dB}$ has been proposed based on simulations as well as measurements. However, such low SIR threshold in [6] has been attained assuming a virtually noise-free environment. In either cases, a constant SIR threshold overlooks the inter-related impact of noise and interference on the LoRa BER performance and correspondingly the LoRa coverage behavior under same SF interference.

In this paper, a numerical approximation of BER performance of LoRa modulation as a function of both SNR and SIR is provided. The analysis starts by deriving an upper bound on cross-correlation interference between two LoRa signals using the same spreading factor. The cross-correlation bound is then employed in approximating the correlation outputs of a typical LoRa receiver from which BER performance is then derived. It is to be noted that BER curves of LoRa in absence of interference could be attained from classical analysis of the optimal detection and error probability for orthogonal signaling [7] (sec. 4.4 p. 203). However, to the best of the authors' knowledge, BER of LoRa under same SF interference is yet to be analytically derived. Comparison between numerical and simulation results indicates that the presented approximation for BER performance is quite accurate. Moreover, simulation of LoRa networks with uniformly distributed end-devices reveals that the approaches adopted in the literature of using a constant SIR threshold of $6\,\mathrm{dB}$ to declare coverage may significantly underestimate the coverage probability of LoRa signals under same SF interference.

The rest of this paper is organized as follows. Section II, reviews the basics of LoRa modulation. An upper bound on cross-correlation interference for two LoRa signals using the same spreading factor is derived in

978-1-5386-6009-6/18/$31.00 ©2018 IEEE

Section III. The derived bound is then deployed in approximating the LoRa correlator outputs on route to deriving the underlying BER performance of LoRa under same SF interference. Section, IV evaluates the accuracy of the BER analysis by comparing it against simulations. The impact of same SF interference on LoRa coverage probabilities is also investigated. Finally, Section V is dedicated for conclusions.

II. Basics of LoRa Chirp Modulation

LoRa adopts a frequency shift chirp modulation scheme [2]. Consider a LoRa system in the baseband where the chirp signal frequency has bandwidth B. Consequently, one LoRa sample is transmitted every $T = 1/B$. LoRa modulation is achieved by spreading the frequency change of the chirp signal across 2^{SF} samples within a symbol duration of $T_S = 2^{SF} \times T$, where $SF \in \{7, 8, ..., 12\}$ depicts the spreading factor. Let $\omega_0(nT)$ depict a basis chirp signal whose frequency increases linearly between 0 and bandwidth B. Accordingly, $\omega_0(nT)$ could be expressed as

$$\omega_0(nT) = \sqrt{\frac{1}{2^{SF}}} \exp\left[j2\pi \cdot (\frac{nB}{2^{SF}}) \cdot nT\right] = \sqrt{\frac{1}{2^{SF}}} \exp\left[j2\pi \cdot (n) \cdot \frac{n}{2^{SF}}\right], \quad (1)$$

where $n = 0, 1, 2, \ldots, 2^{SF} - 1$ depicts the sample index at time nT. For each spreading factor SF in LoRa, 2^{SF} non-binary symbols $s_k = k$, $k \in \{0, 1, 2, \ldots, 2^{SF} - 1\}$ are transmitted using the k^{th} cyclic frequency shift of $\omega_0(nT)$ around the bandwidth B. Accordingly, LoRa specifies a total of 2^{SF} basis signals $\omega_k(nT)$ given as

$$\omega_k(nT) \; = \; \exp\left[j2\pi \cdot (k+n) \mod 2^{SF} \cdot \frac{n}{2^{SF}}\right]. \quad (2)$$

LoRa demodulation is founded on orthogonality of the underlying basis signals [2], where cross-correlation properties between the 2^{SF} possible LoRa basis signals are governed by

$$\mathcal{C}_{l,k} = \sum_{n=0}^{2^{SF}-1} \omega_l(nT) \cdot \omega_k^*(nT) = \begin{cases} 1 & k = l \\ 0 & k \neq l \end{cases}, \quad (3)$$

where $\mathcal{C}_{l,k}$ depicts the cross-correlation between the basis signals $\omega_l(nT)$, $\omega_k(nT)$ $\forall l, k \in \{0, 1, 2, \ldots, 2^{SF} - 1\}$ and $\omega_k^*(nT)$ depicts the complex conjugate of the basis function $\omega_k(nT)$.

Let us assume transmission of a LoRa symbol $s_l = l \in \{0, 1, 2, ..., 2^{SF} - 1\}$ using the basis signal $\omega_l(nT)$ over an AWGN channel. The correlator at the LoRa receiver would generate 2^{SF} outputs corresponding to the correlation of the received signal $r(nT)$ with all 2^{SF} basis signals $\omega_k(nT)$ such that the correlator output $\mathcal{R}_k$ at output bin index k would be given as

$$\mathcal{R}_k = \sum_{n=0}^{2^{SF}-1} r(nT) \cdot \omega_k^*(nT) = \begin{cases} \sqrt{E_S} + \eta_l & k = l \\ \eta_k & k \neq l \end{cases}, \quad (4)$$

where E_S is the symbol energy used to transmit the symbol of interest $s_l = l$ and $\eta_k, \forall k \in \{0, 1, 2, \ldots, 2^{SF} - 1\}$ depicts a complex Gaussian noise process.

The detection of LoRa symbols reverts to selection of the index of the LoRa basis signal that has the highest correlation magnitude with the received signal. Therefore, for the received waveform $r(nT)$ that corresponds to a transmitted symbol $s_l = l$, the detected symbol $\tilde{s}$ is computed as

$$\tilde{s} = \arg_k \max\left(\left|\delta_{l,k}\sqrt{E_S} + \eta_k\right|\right), \quad (5)$$

where, $\delta_{l,k} = 1$ for $k = l$ and $\delta_{l,k} = 0$ otherwise.

Let us define $\rho_k = |\eta_k|$ as the magnitude of the complex noise envelope. Given that η_k is a complex zero-mean Gaussian noise process, then ρ_k depicts a Rayleigh distributed random variable with the cumulative distribution function

$$F_{\rho_k}(\rho) = 1 - \exp\left[-\frac{\rho^2}{2\sigma^2}\right], \quad (6)$$

where $\sigma^2 = N_0/2$ and N_0 is the single-sided noise power spectral density.

Let us define $P_{e|l}$ as the conditional probability of symbol error given that $s_l = l$ is transmitted. Given the outputs of the correlation process defined in (4), $P_{e|l}$ can be expressed as

$$P_{e|l} = \Pr\left[\max_{k,k\neq l}(\rho_k) > \beta_l\right], \quad (7)$$

where $\beta_l = \left|\sqrt{E_S} + \eta_l\right|$ and β_l accordingly follows the Rician distribution with the shape parameter $\kappa_\beta = E_S/2\sigma^2 = E_S/N_0$.

Let $\hat{\rho} = \max_{k,k\neq l}(\rho_k)$ depict a random variable for the maximum of $2^{SF} - 1$ identically distributed Rayleigh random variables. The cumulative distribution function for $\hat{\rho}$ can be given as

$$F_{\hat{\rho}}(\rho) = \left[1 - \exp\left[-\frac{\rho^2}{2\sigma^2}\right]\right]^{2^{SF}-1}. \quad (8)$$

Given (7), (8) and assuming equally probable symbols, the average bit error probability P_b can be expressed as

$$P_b = 0.5 \times \int_0^\infty \left[1 - \left[1 - \exp\left[-\frac{\beta^2}{2\sigma^2}\right]\right]^{2^{SF}-1}\right] \cdot f_\beta(\beta) d\beta, \quad (9)$$

where $f_\beta(\beta)$ is the probability density function for the Rician distributed β. The multiplier of 0.5 before the integral reflects the fact that in LoRa modulation, for each symbol error only half of the underlying symbol bits are expected to be in error. Figure 1 shows the numerical evaluation of the BER performance in (9) as a function of the SNR Γ that is related to E_S/N_0 using

$$\Gamma = \frac{E_s/T_S}{N_0 \cdot B} = \frac{E_S}{N_0 \cdot 2^{SF}}. \quad (10)$$

Table I depicts the announced LoRa sensitivities operating within a bandwidth of $B = 125\,\text{KHz}$ and corresponding to a coding rate of $4/5$ as per [8]. The sensitivities from [8] are mapped to SNR in Table I using the relation $SNR = P_{Rx} + 174 - 10.\log_{10}(B) - NF$ where P_{Rx} is the receiver sensitivity and $NF = 6\,\text{dB}$ is the noise figure [8]. By comparing the SNR values in Table I against the BER curves in Figure 1, it is clear that the reported sensitivities coincide with a BER performance at the scale of $P_b = 10^{-5}$. Accordingly, this shall be used throughout the paper as the metric for coverage evaluation. Table I also includes an additional column holding the exact thresholds $\Gamma_{th}^{(SF)}$ that correspond to a BER performance of 10^{-5} for all spreading factors SF.

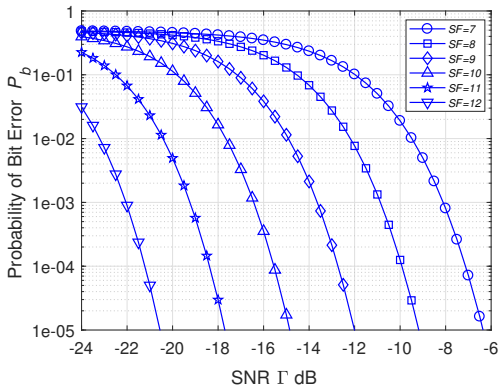

Fig. 1. LoRa BER Performance at different Spreading Factors SF.

TABLE I
SENSITIVITY THRESHOLDS FOR LORA WITH $B = 125$ KHZ, CODING RATE $4/5$.

SF	P_{Rx} [8]	SNR (dB)	$\Gamma_{th}^{(SF)}$ (dB) $P_b \leq 10^{-5}$
7	-123	-6	-6.35
8	-126	-9	-9.15
9	-129	-12	-12
10	-132	-15	-14.8
11	-134.5	-17.5	-17.65
12	-137	-20	-20.55

III. LORA BER PERFORMANCE WITH SAME SF INTERFERENCE

Let us consider a LoRa basis signal of interest $\omega_l(nT)$, $l \in \{0, 1, 2, ..., 2^{SF}\}$ that is interfered with by some other LoRa signal that is using the same spreading factor SF. Since transmitters in LoRa are not synchronized, a random shift of τ samples occurs between the symbol transmission of $\omega_l(nT)$ and any interfering signal. Accordingly, let us define an interference LoRa signal $Z(z_1, z_2, \tau, nT)$ that interferes with $\omega_l(nT)$ to be expressed as

$$Z(z_1, z_2, \tau, nT) = \begin{cases} \frac{1}{\sqrt{\gamma}}.\omega_{z_1}(nT) & 0 \leq n < \tau \\ \frac{1}{\sqrt{\gamma}}.\omega_{z_2}(nT) & \tau \leq n < 2^{SF} \end{cases}, \quad (11)$$

where due to the shift of τ samples between the two transmitters, $\omega_l(nT)$ is effectively exposed to interference from two basis signals $\omega_{z_1}(nT)$, $\omega_{z_2}(nT)$, $z_1, z_2 \in \{0, 1, 2, ..., 2^{SF} - 1\}$ (due to two consecutive interfering LoRa symbols) during the first τ, last $2^{SF} - \tau$ samples of $\omega_l(nT)$, respectively[1]. For an interferer generating equiprobable LoRa symbols, z_1, z_2 in $Z(z_1, z_2, \tau, nT)$ would also follow uniform distributions between 0 and $2^{SF} - 1$. Moreover, the interference $Z(z_1, z_2, \tau, nT)$ is assumed to result in an SIR of γ with respect to the signal of interest $\omega_l(nT)$ that features a normalized symbol energy of 1.

Without loss of generality, let us assume that $0 \leq \tau \leq 2^{SF-1}$ such that the number of interfering samples from $\omega_{z_2}(nT)$ on the signal of interest $\omega_l(nT)$ exceeds those from $\omega_{z_1}(nT)$. Furthermore, also without loss of generality, let us assume that $z_2 = 0$ such that the last $2^{SF} - \tau$ samples of $\omega_l(nT)$ are hit by interference from the basis signal $\omega_0(nT)$. The LoRa demodulator that is synchronized to detect the target signal $\omega_l(nT)$ shall correlate the composite received signal with all basis signals $\omega_k(nT)$. Assuming an AWGN channel, the corresponding correlator outputs $\mathcal{R}_k, \forall k \in \{0, 1, 2, ...2^{SF} - 1\}$ are governed by

$$\mathcal{R}_k = \begin{cases} 1 + \mathcal{I}_l(z_1, \tau) + \eta_l & k = l \\ \mathcal{I}_k(z_1, \tau) + \eta_k & k \neq l \end{cases}, \quad (12)$$

where $\mathcal{I}_k(z_1, \tau), \forall k \in \{0, 1, 2, ..., 2^{SF} - 1\}$ depicts the cross-correlation interference generated by $Z(z_1, 0, \tau, nT)$ at the correlator output bin k while η_k, $k \in \{0, 1, 2, \ldots, 2^{SF} - 1\}$ depict 2^{SF} complex Gaussian noise processes.

Given that the detector selects the symbol $\tilde{s} = \arg_k \max(|\mathcal{R}_k|)$, it becomes necessary to evaluate the magnitudes $|\mathcal{I}_k(z_1, \tau)|, \forall k$ in order to be able to assess the impact of the interfering signal $Z(z_1, 0, \tau, nT)$ on the expected LoRa BER performance. The cross-correlation interference $\mathcal{I}_k(z_1, \tau)$ at each correlator output bin k could be derived from the partial cross-correlation properties of the constituent basis signals $\omega_{z_1}(nT)$, $\omega_0(nT)$ that compose $Z(z_1, 0, \tau, nT)$ with the basis signal $\omega_k(nT)$ that is used for correlation at output bin k. Accordingly, $\mathcal{I}_k(z_1, \tau)$ could be expressed as

$$\mathcal{I}_k(z_1, \tau) = \frac{1}{\sqrt{\gamma}} \times \left(\mathcal{C}_{k,z_1}|_0^{\tau-1} + \mathcal{C}_{k,0}|_\tau^{2^{SF}-1} \right), \quad (13)$$

where $\mathcal{C}_{k,z}|_a^b$ depicts the cross-correlation between the LoRa basis signals $\omega_k(nT)$ and $\omega_z(nT)$ from sample index a to sample index b of $\omega_k(nT)$. The partial cross correlations in (13) could be expanded as

$$\mathcal{C}_{k,z_1}|_0^{\tau-1} = \frac{1}{2^{SF}} \times \sum_{n=0}^{\tau-1} \exp\left[j2\pi \cdot (k - z_1) \cdot \frac{n}{2^{SF}} \right], \quad (14)$$

$$\mathcal{C}_{k,0}|_\tau^{2^{SF}-1} = \frac{1}{2^{SF}} \times \sum_{n=\tau}^{2^{SF}-1} \exp\left[j2\pi \cdot (k) \cdot \frac{n}{2^{SF}} \right]. \quad (15)$$

Given that the summation term in (14) features a geometric series, $\mathcal{C}_{k,z_1}|_0^{\tau-1}$ could be re-formulated as

$$\mathcal{C}_{k,z_1}|_0^{\tau-1} = \frac{1}{2^{SF}} \times \left(\frac{1 - \exp\left[j2\pi \frac{k - z_1}{2^{SF}} . \tau \right]}{1 - \exp\left[j2\pi \frac{k - z_1}{2^{SF}} \right]} \right). \quad (16)$$

By employing the Euler formula for the complex exponentials in (16) followed by using some basic trigonometry, it is possible to prove the following relation for the magnitude of the partial cross-correlation $\mathcal{C}_{k,z_1}|_0^{\tau-1}$ to be given as

$$\left| \mathcal{C}_{k,z_1}|_0^{\tau-1} \right| = \frac{1}{2^{SF}} \times \left| \frac{\sin\left(\pi \frac{k - z_1}{2^{SF}} . \tau \right)}{\sin\left(\pi \frac{k - z_1}{2^{SF}} \right)} \right|. \quad (17)$$

Similarly by following the same steps, it is possible to derive the expression for $|\mathcal{C}_{k,0}|_\tau^{2^{SF}-1}$ to be given as

$$\left| \mathcal{C}_{k,0}|_\tau^{2^{SF}-1} \right| = \frac{1}{2^{SF}} \times \left| \frac{\sin\left(\pi \frac{k}{2^{SF}} . \left(2^{SF} - \tau \right) \right)}{\sin\left(\pi \frac{k}{2^{SF}} \right)} \right|. \quad (18)$$

Given the definition of $\mathcal{I}_k(z_1, \tau)$ in (13) and by using the triangle inequality over constituent partial correlation magnitudes in (17), (18), an upper bound $\mathcal{U}_k(z_1, \tau)$ on the magnitude of cross-correlation interference $|\mathcal{I}_k(z_1, \tau)|$ generated by $Z(z_1, 0, \tau, nT)$ at the correlator output bin k could be given as

[1]For the case of $\tau = 0$, $\omega_l(nT)$ will be exposed to only one interfering basis signal $\omega_{z_2}(nT)$

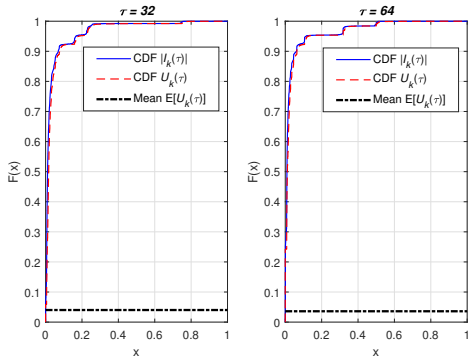

Fig. 2. Cumulative distribution function of cross-correlation interference magnitude $|\mathcal{I}_k(\tau)|$ and upper bound $\mathcal{U}_k(\tau)$ at shifts $\tau = 32,\ 64$.

$$|\mathcal{I}_k(z_1,\tau)| \le \mathcal{U}_k(z_1,\tau) = \frac{1}{2^{SF}.\sqrt{\gamma}} \times \left[\left|\frac{\sin\left(\pi\frac{k-z_1}{2^{SF}}.\tau\right)}{\sin\left(\pi\frac{k-z_1}{2^{SF}}\right)}\right| + \left|\frac{\sin\left(\pi\frac{k}{2^{SF}}.\left(2^{SF}-\tau\right)\right)}{\sin\left(\pi\frac{k}{2^{SF}}\right)}\right|\right] \quad (19)$$

For an interferer generating equi-probable LoRa symbols, z_1 in $Z(z_1,0,\tau,nT)$ also follows a uniform distribution between 0 and $2^{SF}-1$. Accordingly, let $\mathcal{I}_k(\tau)$ depict a random variable for the cross-correlation interference that is experienced at the output correlator bin k assuming τ samples of shift between the signal of interest and the interfering signal. From (13) in conjunction with (17), (18), it is evident that $\mathcal{I}_k(z_1,\tau)$, $k \in \{0,1,2,..,2^{SF}-1\}$ depict 2^{SF} cyclic shifts of each other. Accordingly, the magnitudes $|\mathcal{I}_k(\tau)|$, $\forall k$ would feature 2^{SF} identically distributed random variables. It is to be noted however that these variables while having an identical distribution remain to be dependent. Similarly, let us also define $\mathcal{U}_k(\tau) \ge |\mathcal{I}_k(\tau)|$, $k \in \{0,1,2,..,2^{SF}-1\}$ as 2^{SF} identically distributed random variables that represent the upper bound on the magnitude of cross-correlation interference at any output bin k. Figure 2 compares the cumulative distribution functions for $|\mathcal{I}_k(\tau)|$ and the bound $\mathcal{U}_k(\tau)$ at $\tau = 32,\ 64$ and assuming an SIR $\gamma = 0\,\mathrm{dB}$. The figure indicates that the derived bound is quite tight. Accordingly, we shall from this point utilize the bound $\mathcal{U}_k(\tau)$ to represent the cross-correlation interference behavior across all output correlator bins. Figure 2 also shows horizontal reference lines that correspond to the expectation of the random variable $\mathcal{U}_k(\tau)$ at $\gamma = 0\,\mathrm{dB}$. It is evident that the mean of cross-correlation interference magnitude at each correlator bin k is relatively low when compared to that of the cross-correlation output corresponding to the signal of interest $\omega_l(nT)$ that has a normalized magnitude set to 1. It is also important to emphasize that the mean of cross-correlation interference magnitudes become even lower at more relevant SIR values of $\gamma > 0\,\mathrm{dB}$.

In light of these observations from Figure 2, let us assume that the correlated random variables $\mathcal{U}_k(\tau)$, $k \in \{0,1,2,..,2^{SF}\}$ exhibit a peak cross-correlation interference at some bin $\hat{k} = \arg_k \max(\mathcal{U}_k(z_1,\tau))$ for each realization of z_1 and τ. The cross-correlation interference over the remaining bins $k \ne \hat{k}$ are assumed to be negligible such that $\mathcal{U}_k(z_1,\tau)$ is approximated as

$$\mathcal{U}_k(z_1,\tau) \approx \begin{cases} \mathcal{U}_{\hat{k}}(z_1,\tau) & k = \hat{k} \\ 0 & k \ne \hat{k} \end{cases}. \quad (20)$$

It is evident from (17) and (18) that both $|\mathcal{C}_{k,z_1}|_0^{\tau-1}|$ and $|\mathcal{C}_{k,0}|_\tau^{2^{SF}-1}|$ are governed by the function $\sin(mx)/\sin(x)$ which has a maximum of m at $x = 0$. Consequently, the maxima for each of $|\mathcal{C}_{k,z_1}|_0^{\tau-1}|$ and $|\mathcal{C}_{k,0}|_\tau^{2^{SF}-1}|$ occur at output bin $k = z_1$ with a value of $\tau/2^{SF}$ and at bin $k = 0$ with a value of $\left(2^{SF}-\tau\right)/2^{SF}$, respectively. Therefore, assuming $0 \le \tau \le 2^{SF-1}$, the expression for $\mathcal{U}_k(z_1,\tau)$ in (19) suggests that the peak cross-correlation interference most likely occurs at bin $\hat{k} = 0$, $\forall z_1, \tau$ and the corresponding peak cross-correlation interference for each realization of z_1 and τ is approximated as

$$\mathcal{U}_{\hat{k}}(z_1,\tau) \approx \mathcal{U}_0(z_1,\tau) = \frac{1}{2^{SF}.\sqrt{\gamma}} \times \left[2^{SF} - \tau + \left|\frac{\sin\left(\pi\frac{-z_1}{2^{SF}}.\tau\right)}{\sin\left(\pi\frac{-z_1}{2^{SF}}\right)}\right|\right]. \quad (21)$$

Given the approximations in (20) and (21), the magnitude of the correlator outputs when receiving a signal of interest $\omega_l(nT)$ that is interfered by $Z(z_1,0,\tau,nT)$ could be then approximated as

$$|\mathcal{R}_k|l=0| \approx \begin{cases} |1+\mathcal{U}_0(z_1,\tau)+\eta_0| & k = 0 \\ |\eta_k| & k \ne 0 \end{cases}, \quad (22)$$

$$|\mathcal{R}_k|l\ne 0| \approx \begin{cases} |\mathcal{U}_0(z_1,\tau)+\eta_0| & k = 0 \\ |1+\eta_l| & k = l \\ |\eta_k| & k \ne 0, l \end{cases}, \quad (23)$$

where the approximations in (22) and (23) distinguish between two scenarios when the peak cross-correlation interference coincides with the signal of interest at correlator bin $l = 0$ and when the signal and peak interference appear at different bin outputs for $l \ne 0$, respectively. Accordingly, the probability of symbol error P_e could be evaluated in terms of the conditional probabilities $P_{e|l=0}$ and $P_{e|l\ne 0}$ such that

$$P_e = \frac{1}{2^{SF}} \times P_{e|l=0} + \frac{2^{SF}-1}{2^{SF}} \times P_{e|l\ne 0}. \quad (24)$$

Given that in LoRa $SF \ge 7$ and since for the case of $l \ne 0$ the cross-correlation interference appears on a separate bin than that of the signal of interest, let us assume that the BER performance will be dominated by the scenario $l \ne 0$ with the correlator outputs approximated as per (23). The magnitudes in (23) suggest that the bit error probability P_b for any LoRa signal of interest that is affected by an interference signal with the same spreading factor could be expressed in terms of noise-driven and interference-driven probabilities $P_e^{(N)}$ and $P_e^{(I)}$, respectively, such that

$$P_b = 0.5 \times \left(P_e^{(N)} + \left(1 - P_e^{(N)}\right).P_e^{(I)}\right). \quad (25)$$

The noise driven constituent $P_e^{(N)}$ in (25) reflects the probability that the maximum of the Rayleigh distributed correlator outputs in (23) is greater than $|1+\eta_l|$. Accordingly, similar to (9), $P_e^{(N)}$ is given as

$$P_e^{(N)} = \int_0^\infty \left[1 - \left[1 - \exp\left[-\frac{\beta^2}{2\sigma^2}\right]\right]^{2^{SF}-2}\right] \cdot f_\beta(\beta) d\beta, \quad (26)$$

where the exponent $2^{SF}-2$ depicts the total number of noise-limited outputs in (23) while $f_\beta(\beta)$ remains to represent the probability density function for the Rician distributed output at bin index l. It has been

shown in [9] that the Rician distribution with a shape parameter exceeding 10 dB may be approximated using a Gaussian distribution. Figure 1 in conjunction with (10) suggests that LoRa typically operates within the range of $E_S/N_0 > 15\,\text{dB}$ in order to secure coverage and guarantee a BER performance that is better than 10^{-5}. Accordingly, the Rician distribution $f_\beta(\beta)$ in (26) may be approximated using a Gaussian distribution such that

$$f_\beta(\beta) = \frac{1}{\sqrt{2\pi\sigma^2}} \exp\left[-\frac{(\beta-1)^2}{2\sigma^2}\right], \quad (27)$$

where the mean and variance of β are equal to 1 and $\sigma^2 = N_0/2$, respectively.

For the interference-driven probability of symbol error $P_e^{(I)}$, we shall maintain the assumption that the Rician distributed $|\mathcal{U}_0(z_1,\tau)+\eta_0|$ (given that $\mathcal{U}_0(z_1,\tau)$ depicts the peak cross-correlation interference) operates at a relatively high shape parameters such that it is approximated as a Gaussian distribution with a mean of $\mathcal{U}_0(z_1,\tau)$ from (21) and a variance of $\sigma^2 = N_0/2$. Accordingly, given τ and z_1 that are both uniformly distributed between 0, 2^{SF-1} and between 0, $2^{SF}-1$, respectively, the interference-driven probability of symbol error $P_e^{(I)}$ could be approximated as

$$P_e^{(I)} \approx \frac{\sum_{\tau=0}^{2^{SF-1}} \left[\frac{1}{2^{SF}} \cdot \sum_{z_1=0}^{2^{SF}-1} Q\left(\frac{1-\mathcal{U}_0(z_1,\tau)}{\sqrt{2\sigma^2}}\right)\right]}{2^{SF-1}+1}, \quad (28)$$

where $\mathcal{U}_0(z_1,\tau)$ follows (21) and with $Q()$ being the Q-function, i.e. the tail distribution function of the standard normal distribution. Finally, by combining (26), (28) in (25) the BER probability of LoRa under same SF interference may be numerically evaluated.

IV. Numerical and Simulation Results

The BER performance of LoRa modulation under same SF interference derived using (26), (28) and (25) is shown in Figure 3 for $SF = 7, 8, ..., 12$ assuming an SIR $\gamma = 6\,\text{dB}$. The presented curves exhibit an extremely high accuracy of the derived approximations when compared to simulation results. Figure 3 also includes reference vertical lines $\Gamma_{th}^{(SF)}, \forall SF \in \{7, 8, ..., 12\}$ depicting the SNR thresholds from Table I. In absence of interference, $\Gamma_{th}^{(SF)}$ represents the SNR threshold that is deemed as necessary in order to guarantee coverage within the corresponding LoRa logical network at a BER performance that is better than 10^{-5}. By comparing these reference values against the thresholds $\Gamma_{th}^{(SF)}$ (6 dB) that could be derived from the BER curves in Figure 3, it is clear that the interference has a measurable impact of reducing the sensitivity of LoRa receivers. Such effect is further evaluated in Figure 4 that shows the required sensitivity thresholds $\Gamma_{th}^{(SF)}(\gamma)$ for $SF = 7$, $SF = 12$ as a function of the SIR γ that is experienced by the LoRa signal of interest. It is also to be noted that $\Gamma_{th}^{(SF)}$ from Table I essentially corresponds to $\Gamma_{th}^{(SF)}(\infty)$. The curves in Figure 4 can be used to distinguish coverage regions that reflect the joint impact of operating SNR Γ and SIR γ on LoRa BER performance under same SF interference. Moreover, it is evident in Figure 4 that approximately for $\gamma > 10\,\text{dB}$, the BER performance of LoRa when exposed to same SF

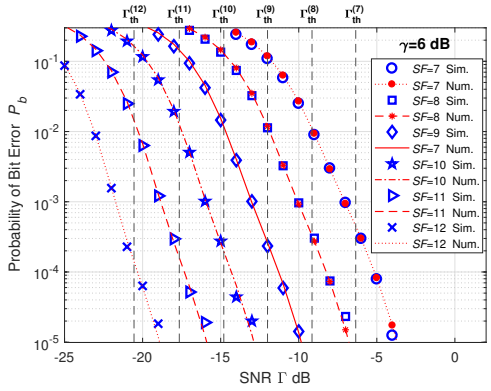

Fig. 3. LoRa BER under Same SF Interference of $\gamma = 6\,\text{dB}$.

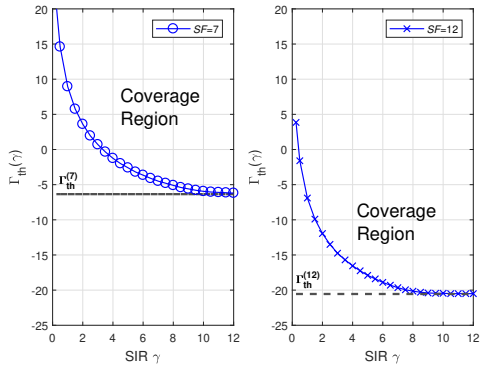

Fig. 4. LoRa SNR Sensitivity Thresholds as a Function of SIR.

interference approaches that of interference free LoRa communication. On other hand, $\Gamma_{th}^{(SF)}(\gamma)$ increases with decreasing γ where it is clear that as γ approaches 0 dB, $\Gamma_{th}^{(SF)}(\gamma)$ increases dramatically. In fact, the curves plotted in Figure 4 start from $\gamma = 0.25\,\text{dB}$. For $\gamma = 0\,\text{dB}$, both the simulation and numerical results have indicated that satisfying the BER requirement of 10^{-5} is not possible within relevant ranges of SNR $\Gamma < \infty$.

In order to investigate the coverage probabilities within LoRa networks, we shall rely on a simulation model that is constituted of six parallel logical networks corresponding to the LoRa spreading factors $SF = 7, 8, ..., 12$. In the simulation model, the coverage region curves for each SF (Figure 4 show these curves for $SF = 7$, $SF = 12$) are used to determine the coverage situation at any given end-device. The simulator adopts a pathloss model with shadow fading that follows

$$PL(d) \propto 10\eta . \log(d) + X_\sigma \quad (29)$$

where $PL(d)$ is the pathloss at a given distance d from the LoRa gateway, η is the pathloss exponent, while X_σ is the shadowing parameter that has a standard deviation of σ_X.

Let us now define a maximum coverage distance $d_C^{(SF)}$ for each SF network that is evaluated assuming $X_\sigma = 0$. In other words, in absence of shadow fading as well as interference, $d_C^{(SF)}$ reflects the maximum distance from the LoRa gateway that guarantees a BER performance that is better than 10^{-5} for an end-device belonging to the corresponding SF network. For an IoT environment with shadowing, setting the SF network

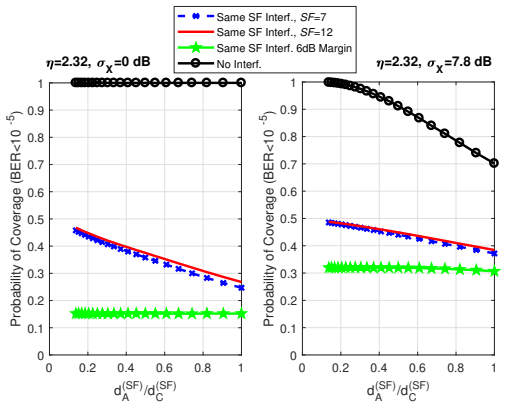

Fig. 5. Probability of Coverage within LoRa Networks.

radius to $d_C^{(SF)}$ would lead to a decrease in coverage probabilities particularly for end-devices that are located towards the edge of the network. Accordingly, let us define an assignment distance $d_A^{(SF)} \leq d_C^{(SF)}$ as the maximum distance from the LoRa gateway within which an end-device is allowed to be assigned with the corresponding spreading factor SF. All end-devices belonging to a given SF network are assumed to be uniformly distributed within the circle determined by the assignment distance $d_A^{(SF)}$. In order normalize our results, we will evaluate all coverage probabilities as a function of the relative radius ratio $d_A^{(SF)}/d_C^{(SF)}$.

Figure 5 presents the coverage probabilities of end-devices within LoRa networks in absence of interference as well as when exposed to same SF interference. The figure considers two IoT environments; a practical environment where the shadow fading parameters follow those derived in [10] with $\eta = 2.32$ and $\sigma_X = 7.8\,\mathrm{dB}$ and a theoretical environment that assumes absence of shadowing with parameters $\eta = 2.32$ and $\sigma_X = 0\,\mathrm{dB}$. The figure also shows coverage probabilities under same SF interference using the conventional approaches adopted in the literature that assume coverage based on SNR thresholds (from Table I) and a constant SIR threshold of $6\,\mathrm{dB}$ that are independent of each other [3], [4], [5], [6]. It is noted from the figures that such criteria for coverage significantly underestimates the coverage probabilities under same SF interference. This is attributed to the fact that in a lot of scenarios with the SIR $\gamma < 6\,\mathrm{dB}$, the device of interest may possibly enjoy a favorable channel between itself and the LoRa gateway such that coverage may still be maintained. Another remark in both presented scenarios is that the behavior of coverage probabilities using the coverage regions derived are virtually similar for all SF networks (only $SF = 7$, $SF = 12$ shown in the figure). This may be explained by referring back to Figure 4 where the sensitivity gap $\Gamma_{th}^{(SF)}(\gamma) - \Gamma_{th}^{(SF)}$ tend to have approximately the same trend for all SF. When shadowing is considered, deceasing the assignment radius increases the coverage probabilities. The rate of increase is more steep for the interference free LoRa transmissions. Moreover, the coverage probability under same SF interference has a maximum of 0.5 since one of the two colliding devices will suffer from inferior SIR (with $\gamma < 0$) and therefore will be considered in outage. For the theoretical scenario, the figures show that in absence of shadowing and interference the coverage as should be expected is maintained at 100% . However, when comparing the coverage probabilities under same SF interference against those for $\sigma_X = 7.8\,\mathrm{dB}$, it is clear that end-devices benefit from the diversity created by the shadowing in achieving better coverage probabilities compared to the case $\sigma_X = 0\,\mathrm{dB}$.

V. Conclusions

In this paper, we have derived a numerical approximation for the LoRa BER performance under same SF interference. Comparison against simulation results reflects the extremely high accuracy of the presented analysis. The BER curves are used to derive coverage regions of SNR and SIR within LoRa networks. Simulation results for coverage probabilities within LoRa networks show that the conventional approaches for assessing coverage based on a constant SIR threshold of $6\,\mathrm{dB}$ significantly underestimates the network performance. In future work, we shall utilize the numerical model in the dimensioning of LoRa networks and determining the assignment radii of each SF network in order to satisfy a given coverage requirement for the IoT applications under study.

Acknowledgment

This work has been supported by the Alexander von Humboldt Foundation in Germany.

References

[1] M. Centenaro, L. Vangelista, A. Zanella, and M. Zorzi, "Long-range communications in unlicensed bands: The rising stars in the IoT and smart city scenarios," *IEEE Wireless Communications*, vol. 23, no. 5, pp. 60–67, 2016.

[2] L. Vangelista, "Frequency shift chirp modulation: The LoRa modulation," *IEEE Signal Processing Letters*, vol. 24, no. 12, pp. 1818–1821, 2017.

[3] O. Georgiou and U. Raza, "Low power wide area network analysis: Can lora scale?" *IEEE Wireless Communications Letters*, vol. 6, no. 2, pp. 162–165, April 2017.

[4] C. Goursaud and J.-M. Gorce, "Dedicated networks for IoT: PHY/MAC state of the art and challenges," *EAI endorsed transactions on Internet of Things*, Oct. 2015. [Online]. Available: https://hal.archives-ouvertes.fr/hal-01231221

[5] J. T. Lim and Y. Han, "Spreading factor allocation for massive connectivity in lora systems," *IEEE Communications Letters*, vol. 22, no. 4, pp. 800–803, April 2018.

[6] D. Croce, M. Gucciardo, S. Mangione, G. Santaromita, and I. Tinnirello, "Impact of lora imperfect orthogonality: Analysis of link-level performance," *IEEE Communications Letters*, vol. 22, no. 4, pp. 796–799, April 2018.

[7] J. G. Proakis and M. Salehi, *Digital communications*, 5th ed. McGraw-Hill, 2008.

[8] Semtech application note an1200.22, "lora modulation basics," revision 2, semtech corporation, may 2015. [Online]. Available: https://www.semtech.com/uploads/documents/an1200.22.pdf

[9] R. D. Nowak, "Wavelet-based Rician noise removal for magnetic resonance imaging," *IEEE Transactions on Image Processing*, vol. 8, no. 10, pp. 1408–1419, 1999.

[10] J. Petajajarvi, K. Mikhaylov, A. Roivainen, T. Hanninen, and M. Pettissalo, "On the coverage of lpwans: range evaluation and channel attenuation model for lora technology," in *2015 14th International Conference on ITS Telecommunications (ITST)*, Dec 2015, pp. 55–59.